Marine Chemistry 275 (2026) 104611

Contents lists available at ScienceDirect

Marine Chemistry

journal homepage: www.elsevier.com/locate/marchem

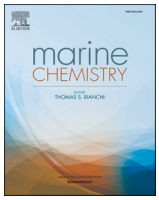

Distributions of particulate Al and Fe in the Bay of Bengal and south Indian subtropical gyre

Pamela M. Barrett [a,*], Joseph A. Resing [a], Maxime M. Grand [b,1], Christopher I. Measures [b], William M. Landing [c]

[a] Cooperative Institute for Climate, Ocean, & Ecosystem Studies, University of Washington and PMEL/NOAA, Seattle, WA, USA
[b] Department of Oceanography, University of Hawaii, Honolulu, HI, USA
[c] Department of Earth, Ocean, and Atmospheric Science, Florida State University, Tallahassee, FL, USA

ARTICLE INFO

Keywords:
Particulate matter
iron
Aluminum
Indian Ocean

ABSTRACT

The trace element composition (Al, Si, P, Ca, and Fe) of suspended particulate matter is presented for the upper 1000 m of the water column along U.S. CLIVAR/CO_2 Repeat Hydrography zonal section I05 (2009) in the South Indian subtropical gyre and meridional section I09N/I08S (2007) in the eastern Indian Ocean from the Bay of Bengal to the subtropical front. Along I09N, high particulate Al and Fe concentrations are found throughout the Bay of Bengal and the northern Indian Ocean indicating significant lithogenic particle loads from river-borne sediment transport and smaller contributions from continental dust flux than current model estimates. Particles have elevated Fe:Al ratios compared to the composition of local shelf sediments, indicating that suspended particulate matter becomes enriched from scavenging of dissolved Fe that accumulates in the oxygen minimum zone in the Bay of Bengal. Along I05, retroflection of the Agulhas Return Current transports African shelf-derived lithogenic particles into the western South Indian basin, resulting in the elevated subsurface concentrations of particulate Al and Fe nearly 3000 km into the interior of the subtropical gyre. Another region of elevated dissolved Fe concentrations and Fe-enriched particulate matter was also observed along I05 in intermediate waters (>600 m) in the subtropical gyre at 32°S between 70 and 74°E, suggesting inputs from a shallow sedimentary or possibly volcanic Fe source to these stations. Comparison of data from the crossover between the I05 and I09N/I08S sections and from the 2007 and 2016 occupations of I09N allows investigation of the temporal variability of basin-scale distributions of particle-associated trace metals with relatively short residence times in the upper water column. The most pronounced differences in trace metal distributions are associated with interannual variability in productive near-coastal and upwelling regions where mixed-layer pFe concentrations vary by a factor of 2–7, whereas Fe and Al in deeper waters and dust-impacted surface waters in oligotrophic regions show significantly less variability.

1. Introduction

The particle phase dominates both fluxes and oceanic reservoirs of many trace metals in the global ocean. Particle dynamics, including processes such as active biological uptake, adsorption/desorption, aggregation, dissolution, and authigenic precipitation are controls on trace metal distributions (Jeandel and Oelkers, 2015). Hence, the distribution and composition of particulate matter impacts both the availability of biologically-important elements (e.g., Fe) and the interpretation of paleoclimate proxies and tracers of modern marine processes (e.g., Al).

The particulate phase may function as both a source and a sink for trace metals (Ye et al., 2011). For example, the distribution of bioavailable dissolved Fe is closely related to the distribution of Fe in the particulate phase, which can represent a large reservoir of labile, exchangeable Fe (e.g., Milne et al., 2017). Particles also typically represent the primary removal mechanism for trace metals in the ocean via active biological uptake and passive scavenging by both lithogenic and biogenic particles. Changes in particle concentration and

* Corresponding author.
E-mail addresses: barrettp@uw.edu (P.M. Barrett), joseph.resing@noaa.gov (J.A. Resing), maxime.grand@sjsu.edu (M.M. Grand), measures@hawaii.edu (C.I. Measures), wlanding@fsu.edu (W.M. Landing).
[1] Now at Moss Landing Marine Laboratories, Moss Landing, CA, USA.

https://doi.org/10.1016/j.marchem.2026.104611
Received 15 October 2025; Received in revised form 23 December 2025; Accepted 22 January 2026
Available online 23 January 2026

composition can result in highly variable removal rates of both micronutrients and biochemical tracers, as demonstrated by challenges determining residence times for Al in efforts to quantify atmospheric dust flux to the surface ocean (e.g., Anderson et al., 2016; Menzel Barraqueta et al., 2019). Further complicating understanding of the role of particles in marine trace metal cycling is uncertainty associated with interpretations of particulate trace metal concentrations as proxies for the presence of different particle components with specific origin (i.e., lithogenic, authigenic, or biogenic) and known composition. Passive scavenging of the dissolved phase has been observed to have localized, but significant impacts on particulate trace metal distributions, leading to unexpected chemical bulk composition in regions with strong bloom cycles in primary productivity (Moran and Moore, 1988; Barrett et al., 2012) or with large advective trace metal inputs (Barrett et al., 2018; Artigue et al., 2021). These open questions about the use of particle tracers and particle regulation of trace metal biogeochemical cycling in the ocean necessitate continued investigation of particulate trace metal distributions in the global ocean. Such datasets will be critical to validate model parameterizations of particle dynamics (e.g., Ye and Völker, 2017), and to test assumptions about particle-mediated processes in trace metal modelling efforts (Dutay et al., 2015; Somes et al., 2021; Tagliabue et al., 2016; Weber et al., 2018; van Hulten et al., 2013, Hulten et al., 2017; Weber et al., 2018; Xu and Weber, 2021). Despite significant advances in model capabilities, current global models are still limited by omitted or overly limited representations of key mechanisms such as non-reductive sedimentary inputs, scavenging by non-biogenic particles, and representation of (ir)reversible scavenging processes, highlighting the need for continued integration of observational datasets to improve model fidelity and predictive skill.

This manuscript presents the trace element composition (Al, Fe, P, Ca, Si) of suspended particulate matter samples collected in the Indian Ocean along zonal CLIVAR I05 section across the subtropical gyre and along the meridional I09N/I08S section from the Bay of Bengal to the subtropical front. The eastern Indian Ocean and South Indian subtropical gyre are characterized by a transition from a biologically productive system with significant fluvial sediment transport and aerosol deposition (Panda et al., 2014) in the Bay of Bengal to an oligotrophic gyre with potentially significant input of particles from continental margin sources but relatively low aeolian trace metal inputs (Grand et al., 2015a). Limited trace metal data has been reported for the Indian Ocean compared to the basin-scale datasets available for other regions (GEOTRACES Intermediate Data Product, 2021), and recent Al and Fe modelling studies report relatively poor fit to observations compared to other basins (Xu and Weber, 2021). High resolution sampling in the upper ocean along these three CLIVAR sections provides an opportunity to determine likely sources for biogenic and lithogenic particles and investigate the processes that drive their cycling. Additionally, the residence time for particle-associated trace metals is generally much shorter than for dissolved species, making current datasets subject to greater uncertainty from potential variability not captured by limited existing observations. Such variation could arise from several factors operating on a range of timescales, such as seasonal to decadal changes in external inputs or variability in biological uptake (e.g., Chan et al., 2024; Sedwick et al., 2005). Here, we examine the distributions of particulate Fe and Al in the Indian Ocean and evaluate the processes that influence them, including dust deposition, continental inputs, biological uptake, and abiotic scavenging. Additionally, comparisons between depth profiles collected at the crossover of the CLIVAR I05 and I09N/I08S sections, as well as between our March 2007 I09N dataset and surface-layer sampling conducted at a subset of I09N stations in April 2016, are used to assess temporal variability in particulate trace metal distributions.

2. Methods

Trace metal sampling was conducted along U.S. CLIVAR/CO_2 Repeat Hydrography sections I09N/I08S (15 February to 26 April 2007) and I05 (24 March to 11 May 2009) (Fig. 1). Typical station spacing was approximately 1 degree of latitude. Seawater was collected from the upper 1000 m using 12 L GO-FLO bottles suspended on a trace metal rosette and subsampled in a clean laboratory van equipped with a HEPA filtered air system (Measures et al., 2008a). Suspended particulate matter (SPM) was collected by pressure-filtering (<55 kPa, filtered compressed air) seawater through acid-washed, 0.4 μm track-etched polycarbonate filters (Millipore). Backing filters of mixed cellulose ester were used for even sample loading in polypropylene filter holders. The average filtration volume was 9 L. Filters were gently rinsed with deionized water adjusted to pH 8 with ammonium hydroxide (3 x ~ 5 mL) with a low vacuum applied while avoiding loss or redistribution of particles in order to remove residual seasalt, avoiding salt interferences in ED-XRF analyses. It is possible that a loss of more labile elements (e.g., pP) could result from the rinse protocol. Past work comparing rinsed SPM metal:P ratios with independent cellular values (e.g., Barrett et al., 2018; Table 2) suggest such impacts may be small; however, we have not done explicit testing of potential rinsing losses. We plan during future sample collection, and encourage others to consider, simple experiments to evaluate this directly so more clear recommendations for differing study aims can be made.

SPM samples were analyzed using energy-dispersive x-ray fluorescence (ED-XRF) on a Thermo Fisher Quant'X under a vacuum atmosphere and calibrated with both commercial thin film standards (MicroMatter) and standards prepared using a modification of the method reported by Holynska and Bisiniek (1976). The full ED-XRF methodology, including an HR-ICPMS intercalibration exercise performed with a subset of I09N samples (Fig. S1), is detailed in Buck et al. (2021). Method blanks, determined from unused, acid-cleaned filters, were subtracted from measured sample values. Values for method blanks and detection limits for elements of interest are reported in Table 1. Analytical accuracy was confirmed by analysis of certified reference material NIST SRM 2783 (air particulate on filter media, Table 1).

Data from the I08S section south of the subtropical front have been discussed in prior work with additional data from the Indian sector of the Southern Ocean (CLIVAR section I06S) (Barrett et al., 2018). Dissolved Fe and Al data have previously been reported for both sections I05 (Grand et al., 2015a) and I09N/I08S (Grand et al., 2015b, 2015c). The particulate and dissolved trace metal datasets from each section are publicly available on the CCHDO website (http://cchdo.ucsd.edu) under Expocodes 33RR20070322 (I09N), 33RR20070204 (I08S), and 33RR20090320 (I05S). The hydrographic data presented in supplemental figures were taken from the main CLIVAR CTD and 36-bottle rosette. Salinity and nutrient samples were drawn from GO-FLO bottles and compared to the main CLIVAR rosette to confirm trip depth; hydrographic data and methodological information are available on CCHDO under the Expocodes listed above.

3. Results and discussion

3.1. Hydrography and surface circulation

The I09N/I08S meridional section extends from 18°N in the Bay of Bengal traversing the central basin over 82–95°E and then continues southwards to the subtropical front along 95°E. The I05 zonal section spans the South Indian subtropical gyre at 30–34°S from the African margin at 30°E to the Australian shelf at 115°E, intersecting the I9N/I08S section at 95°E. A full discussion of general circulation patterns and water masses sampled along the I09N/I08S (Grand et al., 2015c) and I05 sections (Grand et al., 2015a) has been presented previously. Here, we briefly describe the relevant hydrographic context for the particulate trace element distributions. Station locations and a simplified schematic of surface circulation is shown in Fig. 1. Salinity, temperature, dissolved oxygen, and nitrate distributions for both sections are presented in

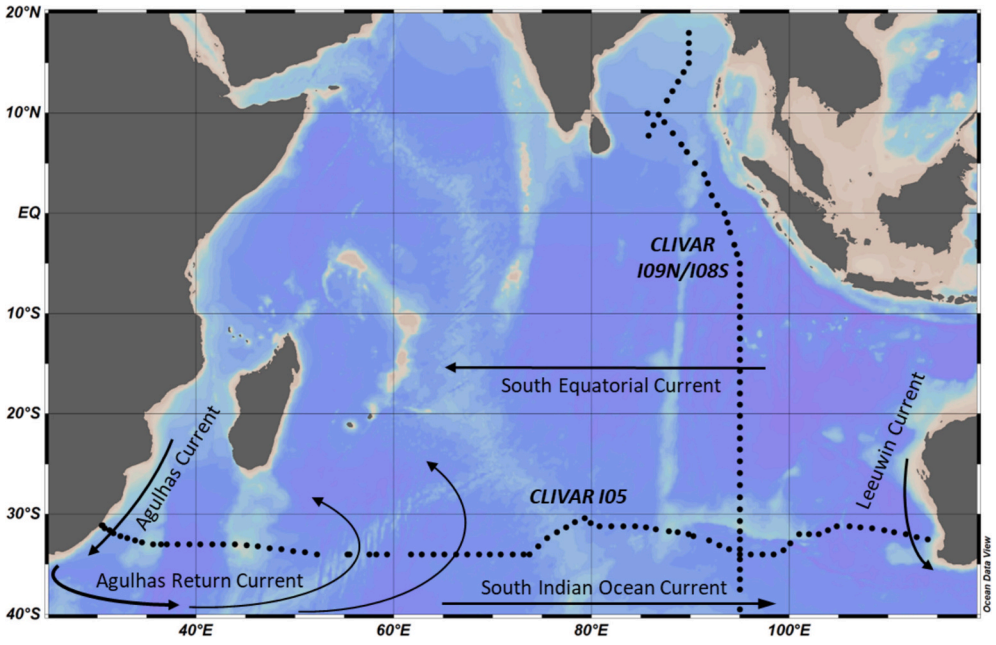

Fig. 1. Location of trace metal sampling stations along CLIVAR zonal section I05 (2009) and meridional section I09N/I08S (2007) north of the subtropical front. Large-scale circulation patterns shown are based on Stramma and Lutjeharms (1997) and near-surface LADCP velocities observed during occupations of the I09N/I08S and I05 sections (Grand et al., 2015a, 2015b, 2015c).

Table 1
Detection limits and method blank values for trace elements of interest as given in filter sample concentrations (ng cm^{-2}) and equivalent seawater concentration (nM) for the max filtration volume (11.2 L) with results of analysis of NIST 2783 (air particulate on filter media) compared to certified values. Where no method blank is given, the signal peak was indistinguishable from the background.

	detection limit		method blank		NIST 2783	
	ng cm^{-2}	nM	ng cm^{-2}	nM	certified value (ng cm^{-2})	measured (ng cm^{-2})
Al	8.9	0.36	14.5	0.6	2330 ± 53	2032 ± 125 (n = 40)
Fe	1.0	0.02	4.32	0.1	2660 ± 160	2945 ± 81 (n = 40)
P	2.0	0.07	41.9	1.5	N/A	N/A
Ca	4.0	0.1	9.25	0.3	1325 ± 110	1269 ± 71 (n = 40)
Si	4.6	0.2	BDL	–	5884 ± 160	5400 ± 440 (*n* = 40)

Fig. S2.

The northern reach of the I09N/I08S meridional section in the Bay of Bengal is approximately 400 km from the mouth of the Ganges-Brahmaputra river delta. The Bay of Bengal receives large fluvial inputs from the Ganges-Brahmaputra river system that are influenced by the Indian Ocean monsoon system. During the northeast monsoon (Dec-Mar), high pressure over the Indian subcontinent leads to northeasterly winds carrying cool, dry and dust-laden air to the Bay of Bengal (Panda et al., 2014). During the southwest monsoon (June-Sept), reversal of winds carries moisture-laden oceanic air masses over the river basin, leading to heavy precipitation and run-off into the Bay of Bengal. Low salinities and high sea surface temperatures lead to highly stratified surface waters and relatively shallow mixed layers (typically <20 m). Although sampling along I09N/I08S occurred at a time of relatively low freshwater discharge prior to the onset of the southwest monsoon (April 2007), a characteristic low-salinity lens was observed in surface waters north of the equator, resulting in strongly stratified surface waters and minimal vertical mixing (Fig. S2). Subsurface waters along I09N/I08S in the Bay of Bengal to 5°N were generally hypoxic (2–60 μmol kg^{-1}) below approximately 150 m and enriched in nitrate (25–40 μmol kg^{-1}) (Fig. S2). Low dissolved oxygen (<200 μmol kg^{-1}) and high nitrate (10–35 μmol kg^{-1}) concentrations were observed in subsurface waters throughout the northern Indian Ocean along I09N/I08S to the South Equatorial Current (SEC) at 15°S (Fig. S2).

The westward-flowing SEC is evident along the I09N/I08S section as a region of sharp transition between low-salinity surface waters overlying the oxygen minimum zone in the Bay of Bengal and Northern Indian Ocean and the high-salinity, well-oxygenated waters of the subtropical gyre (Fig. S2). Anti-cyclonic gyre circulation continues south as the Agulhas Current, the western boundary current flowing along the South African shelf. Along I05, the 5 stations closest to the African margin (west of 31.2°E) are within the Agulhas Current as evident from LADCP data (Grand et al., 2015a). Although some Agulhas waters are carried by eddies into the South Atlantic, the majority of the flow retroflects and rejoins the gyre circulation in the South Indian basin, becoming the Agulhas Return Current. Much of the eastward-flowing water of the Agulhas Return Current is recirculated within the western gyre (Stramma and Lutjeharms, 1997) where it intersects the I05 track. By 70°E, the eastward flow volume is reduced by an estimated 70% (Lutjeharms and Ansorge, 2001), and the remaining flow along the subtropical convergence in the eastern basin continues as the South Indian Ocean Current. In the eastern basin, the I05 cruise track makes northward incursions towards the center of the gyre (to ~30°N) that are apparent in the regions of higher surface salinities and temperature centered at ~80 and ~ 105°E. Circulation in the eastern gyre is relatively weak and lacks a prominent northward-flowing eastern boundary current. Along the Australian margin, the Leeuwin Current flows southward along the shelf; LADCP velocities indicate the I05 station closest to the Australian shelf at 114°E is influenced by the Leeuwin Current.

3.2. I09N/I08S: Bay of Bengal and northern Indian Ocean

Distributions of particulate P, Ca, Si, Al and Fe along the I09N/I08S section are shown in Fig. 2. The biogenic pFe (pFe_{bio}) pool was calculated from observed pP concentrations using a cellular Fe/P quota of 0.6 mmol mol^{-1} and is reported as a percentage of total pFe concentrations.

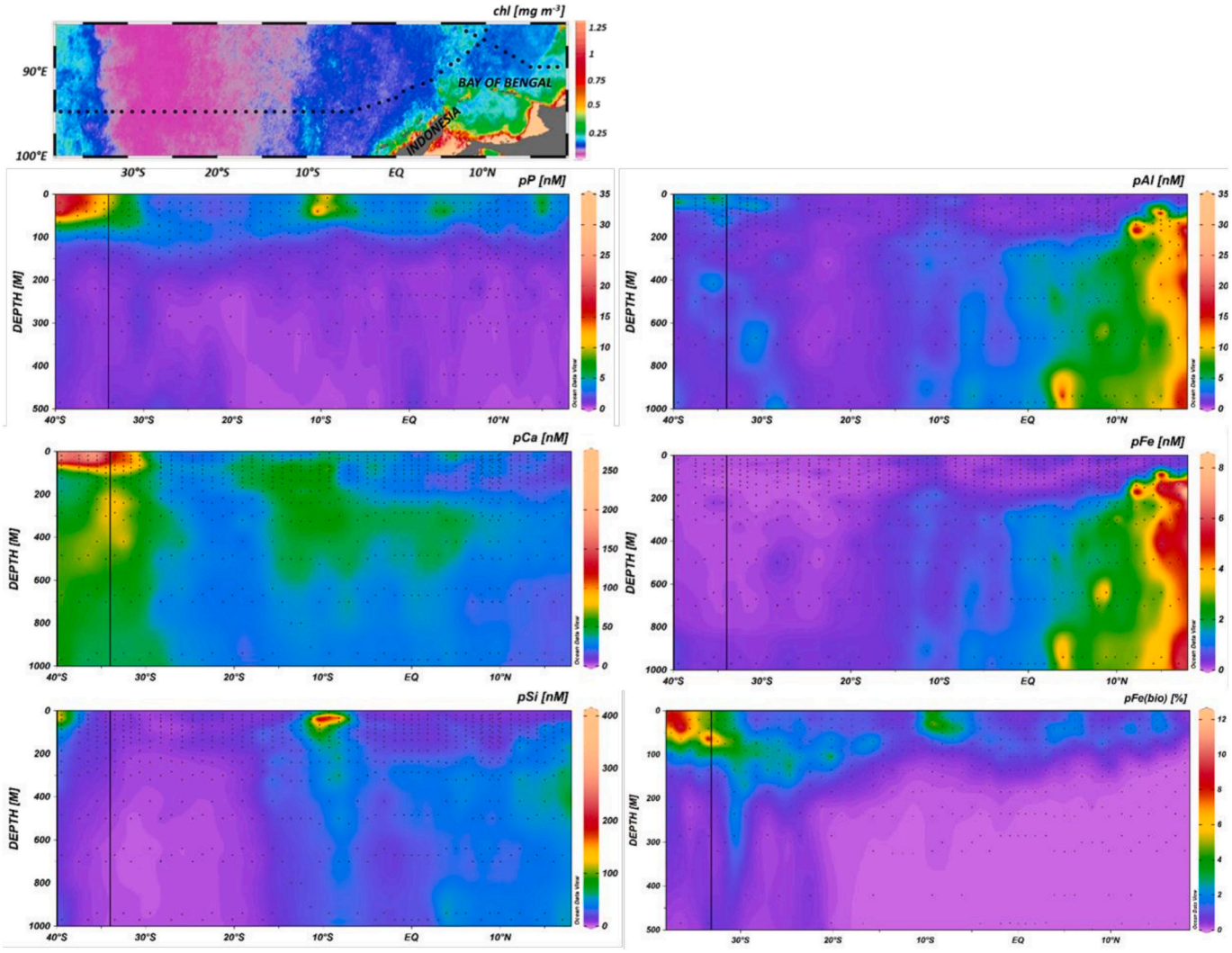

Fig. 2. Distribution of particulate P, Ca, Si, Al, Fe (nM) and pFe_{bio} (%) along CLIVAR section I09N/I08S from the Bay of Bengal to 40°S. Note the reduced depth scale (500 m) in the plots of particulate P and pFe_{bio}. Black points indicate individual samples; the black line at 34°S represents the crossover point with CLIVAR section I05. The top panel shows average chlorophyll concentrations (mg m^{-3}) over Feb-Apr 2007 from SeaWiFS satellite imagery overlaid with the locations of trace metal stations.

The Fe/P quota used is the average value measured in individual phytoplankton cells collected along I09N in 2016 (Twining et al., 2019); differences between cells were not statistically significant. The measured Fe/P quotas along I09N are among the lowest of global observations of marine phytoplankton Fe stoichiometry (Twining and Baines, 2013) and could return a conservative estimate of pFe_{bio}. Note that plots of pP and pFe_{bio} are restricted to the upper 500 m as pP concentrations below this depth were typically below the ED-XRF detection limit (0.1 nM); all other plots extend to 1000 m.

3.2.1. *Biogenic particle distributions: Particulate P, Ca, and Si along I09N/I08S*

Concentrations of particulate P (pP) are highest (up to 30 nM) within the upper 100 m and covary with fluorescence in the upper 200 m ($R^2 = 0.64$), consistent with a biogenic particle source. Rapid attenuation of pP occurs with depth and concentrations are relatively homogenous below 200 m, averaging 0.9 ± 0.8 nM. Concentrations of particulate Ca (pCa) in surface waters arise primarily from production and export of biogenic $CaCO_3$ by coccolithophores. Similarly, production of biogenic silica by diatoms is reflected by mixed-layer particulate Si (pSi) distributions. However, the subsurface distribution of pSi can be dominated by inputs of aluminosilicate minerals rather than export of biogenic particles as observed in the Bay of Bengal and discussed further below.

Although pP is generally low (<5 nM) in surface waters in the Bay of Bengal and Northern Indian Ocean, there are two regions along I09N where concentrations are elevated. The first occurs at 7 stations centered at 10°S where pP concentrations up to 29 nM are observed. Here, open-ocean Ekman pumping results in localized upwelling in a band across the Indian Ocean (Schott et al., 2002). Although this upwelling feature is strongest during the southwest monsoon, it is present throughout the year and is evident during sampling of the I09N/I08S section by shoaling of isotherms and nutriclines at 10°S (Fig. S1). Increased biological productivity from this nutrient delivery to surface waters can be seen by a band of high chlorophyll concentrations in surface waters at ~10°S during occupation of I09N/I08S (Fig. 2); such blooms are frequently observed by ocean color satellite imagery across this upwelling regime (Murtugudde et al., 1999). The sharp increase in pSi (>300 nM) relative to concentrations at surrounding stations in the subtropical gyre (<25 nM) suggests this upwelling-enhanced biological activity is primarily due to increased diatom productivity.

Sharp increases in chlorophyll, pP (up to 19 nM), and pCa (up to 270 nM) in surface waters are also found at the southern edge of the subtropical gyre beginning at 30°S. This region of elevated pCa extends into circumpolar waters and is discussed more extensively in Barrett et al.

(2018). Our observations are consistent with remote sensing algorithms (Balch et al., 2005, 2011; Sadeghi et al., 2012) and in situ studies (Balch et al., 2014; Holligan et al., 2010) that suggest a pattern of high coccolithophore production in a band around the Southern Ocean spanning ~30° to 60°S (the "Great Calcite Belt").

3.2.2. Particulate Al and Fe along I09N/I08S

The subsurface distribution of pAl and pFe in the Bay of Bengal and northern Indian Ocean is strongly influenced by the Ganges-Brahmaputra river system, which is estimated to deliver $>10^8$ tons of suspended sediment annually into the Bay of Bengal (Islam et al., 1999). Sediment loads can vary seasonally by several orders of magnitude according the monsoon cycle in the tropical Indian Ocean; sampling along I09N/I08S occurred in spring, a time of minimum sediment delivery from the river system (Barua et al., 1994). Maximum pAl (35.4 nM) and pFe (13.6 nM) concentrations are observed at northernmost stations in the Bay of Bengal approximately 400 km from the river delta with subsurface maxima at depths of 150–450 m and concentrations generally decreasing with distance offshore, consistent with lateral transport of sediment from the shelf (Fig. S3). The pSi distribution also reflects this large input of lithogenic particles, with a local maximum (~50–85 nM) at these depths coincident with the pFe and pAl signals. The observed Fe:Al molar ratio of suspended particle matter in the subsurface (>150 m) particle plume that extends from the Bay of Bengal to the equator is 0.38 ± 0.05, somewhat higher ($p > 0.01$, two-tailed one-sample t-test) than the composition of suspended sediment sampled over the shelf within 100 km of the river mouth (Fe:Al ratio of 0.27) (Stummeyer et al., 2002), or the Fe:Al of bulk continental crust (0.26) (Wedepohl, 1995). Suspended particulate matter is likely enriched in Fe due to scavenging of the large subsurface reservoir of dFe (0.6–1.5 nM) that accumulates in this region from both sinking organic matter remineralization and sedimentary dFe inputs from the shelf (Grand et al., 2015b; Chinni et al., 2019).

Particulate Al and Fe distributions in the Bay of Bengal are also impacted by deposition of aerosol dust transported from the Indian peninsula and Southeast Asia. Sampling along I09N/I08S took place during peak seasonal dust transport associated with the late NE monsoon (Jan-April) when winds carry continental air masses over the Bay of Bengal (Srinivas and Sarin, 2013). Previous studies have estimated annual dust fluxes of 0.3–6 g m^{-2} yr^{-1} from ship-board observations (Srinivas and Sarin, 2013; Panda et al., 2014), 2.5 g m^{-2} yr^{-1} from surface-ocean dAl measurements (Grand et al., 2015b), and 2–10 g m^{-2} yr^{-1} from atmospheric model output (Ginoux et al., 2001; Zender et al., 2003; Jickells et al., 2005). Given high modelled dust flux estimates, surface waters in the Bay of Bengal had unexpectedly low average mixed-layer pAl (1.0 ± 0.6 nM) and pFe (0.3 ± 0.1 nM) concentrations north of 5°N at the time of sampling. For comparison, concentrations up to an order of magnitude higher (>10 nM pAl and > 3 nM pFe) have been observed in the equatorial North Atlantic under the Saharan outflow (Barrett et al., 2015) where annual dust deposition is estimated at 2–20 g m^{-2} yr^{-1} (Buck et al., 2010; Mahowald et al., 2005; Measures et al., 2008a). The relatively low concentrations observed in the Bay of Bengal could result from a combination of the episodic nature of dust deposition and relatively short residence times (days to weeks) expected for mineral dust particles in the surface ocean (Dammshäuser et al., 2013). However, dry deposition dominates aerosol delivery to surface waters during this period (Srinivas and Sarin, 2013), introducing less temporal variability in flux rates compared to periods with significant wet deposition. Additionally, trace metal sampling during the April 2016 occupation of I09N also revealed similarly low pFe (0.3–0.6 nM) and pAl (0.6–2.5 nM) concentrations in Bay of Bengal surface waters (Twining et al., 2019), giving confidence that our observations were representative of typical conditions in this region. Assuming steady-state conditions with observed mixed layer depth (50 m), Al content of aerosol dust (8%), and estimated residence of particles in the mixed layer (several days), we determine that the observed surface ocean pAl distribution could originate from a dust flux of ~2 g m^{-2} yr^{-1}. Because sampling occurred during the high dust season and a short residence time was chosen for calculations, on this value represents an upper limit on the dust flux. Hence, our observations are most consistent with dust deposition estimates based on direct atmospheric sampling and steady-state models of dAl distributions, and on the lower end of atmospheric model estimates.

South of the SEC in the South Indian subtropical gyre, pAl concentrations are generally low in the upper 1000 m (0.4–2.0 nM) and average 1.2 ± 0.8 nM in surface waters. These surface-ocean observations are generally consistent with concentrations that would be expected from recent estimates of dust flux to subtropical waters of 0.5 ± 0.3 g m^{-2} yr^{-1} (Grand et al., 2015b), using similar assumptions of mixed layer depth and residence time detailed above. However, there are two regions at ~10°S and south of 30°S where elevated pAl concentrations are found in surface waters; these coincide with the regions of high biological productivity discussed above. The high pAl signal (up to 3.7 nM) centered at 10°S likely arises from scavenging of the relatively high dAl concentrations in these surface waters by Si-rich particles in this upwelling zone, passive adsorptive scavenging by diatoms being a significant sink in the cycling of dAl (Hydes, 1979; Orians and Bruland, 1986). Here, there could also be a contribution of pAl from a remnant sedimentary signal in the Indonesian Throughflow that is the source of high surface-ocean dAl here (Grand et al., 2015c). South of ~30°S, elevated surface-ocean pAl concentrations up to 12.4 nM are associated with elevated pCa in the band of high coccolithophore productivity that begins at the southern edge of the subtropical gyre. As discussed in Barrett et al. (2018), this pAl signal is largely due to passive scavenging of dAl by biogenic $CaCO_3$-rich particles rather than onto diatom frustules. The mixed layer dAl pool at these latitudes is in part supplied by local dust deposition but is estimated to be largely supplied (>75%) by the lateral advection of Al-rich waters from the western gyre (Barrett et al., 2018).

Concentrations of total pFe are relatively low in the central South Indian Gyre, averaging 0.13 ± 0.03 nM in the surface layer (I09N/I08S stations 70–113). The portion of the pFe pool associated with biogenic particles along the transect is estimated to be a maximum of 16% in productive surface waters; using the full range of measured values from Twining et al. (2019) would return a maximum of 8–17% pFe_{bio}. Biogenic pFe generally declines with depth and is notably <0.1% of total pFe concentrations in subsurface waters >200 m in the Bay of Bengal. Higher concentrations of surface-ocean pFe (0.5–0.9 nM) and an increased proportion of pFe_{bio} are found at 5 stations (stations within the localized upwelling feature centered at centered at 10°S, associated with a shallow nutricline (Fig. S2) and the elevated signals seen in satellite chlorophyll, pP, and pSi (Fig. 2). Indicators of primary productivity (chlorophyll, pP and pCa) also increase south of ~30°S as the section approaches the subtropical front and the northern extent of the Southern Ocean calcite belt. Here we find the highest contributions of pFe_{bio} to the total pFe pool but little increase in total measured pFe as lithogenic pFe inputs from aerosol dust deposition significantly decline south of 30°S (Grand et al., 2015b).

3.2.3. Data comparison with 2016 I09N trace metal sampling

Suspended particulate matter samples were collected in the surface layer (generally 20 m) at a subset of stations during an April 2016 occupation of I09N (Twining et al., 2019). The concentrations of pFe and pAl in surface waters from both March 2007 and April 2016 are plotted in Fig. 3. Although sample collection, processing, and analysis varied (ED-XRF analysis of polycarbonate filters in this study; sequential digestion followed by HR-ICP-MS analysis of Supor filters by Twining and coauthors), the pFe and pAl datasets show similar latitudinal trends in surface-ocean concentrations. As will be discussed further below when considering the depth profiles at the I09N/I08S and I05 crossover stations, the largest differences in particulate trace metal concentrations primarily stem from interannual variability in biological productivity. Both datasets show increasing concentrations of both pFe and pAl

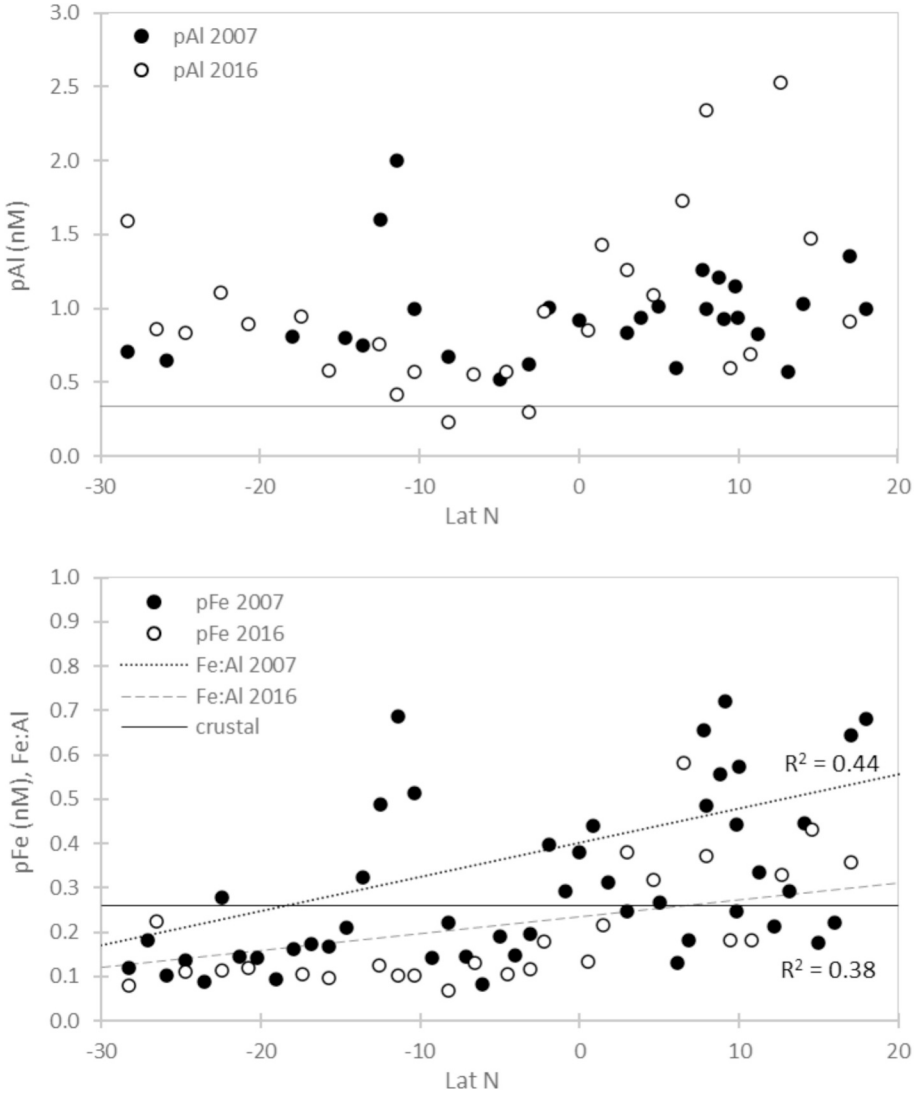

Fig. 3. Concentration of pAl (top panel) and pFe (bottom panel) in surface-layer samples along I09N in March 2007 (solid symbols, 8–25 m, this study; analyzed by ED-XRF) and in April 2016 (open symbols, 18–40 m, Twining et al., 2019; analyzed by HR-ICP-MS). The plot of pAl is shown with a solid vertical line representing the analytical limit of detection for the ED-XRF data (this study only). The solid vertical line in the pFe plot represents bulk crustal Fe:Al of 0.26 (Wedepohl, 1995) while dotted lines show latitudinal trends in particle Fe:Al measured in 2007 ($R^2 = 0.44$) and 2016 ($R^2 = 0.31$).

northwards into the Bay of Bengal, although pFe concentrations measured in 2009 were generally higher and pAl concentrations measured in 2016 were more variable. The largest differences are pFe concentrations that were up to 7× times higher in 2007 than measured in 2016 at the upwelling region centered at 10°S. The 2016 dataset does not show an elevated pFe signal (or associated scavenged pAl) due to increased productivity, although Twining and coauthors do report elevated particulate Zn concentrations here that they attribute to increased phytoplankton biomass and response in biogenic particle composition. Outside of the Bay of Bengal and this upwelling zone, open-ocean pAl and pFe concentrations are very similar in the North Indian Ocean and South Indian subtropical gyre during the two occupations of I09N. Difference in average Fe:Al between 2007 (0.40 ± 0.15) and 2016 (0.22 ± 0.9) are largely driven by Fe-enriched particles in 2007 in those two regions, and both datasets show a weak trend of increasing Fe:Al in surface particles from the subtropical gyre into the Bay of Bengal (Fig. 3).

3.3. I05: South Indian subtropical gyre

Distributions of pP, pCa, pSi, pAl, pFe, and pFe_{bio} along the I05 zonal section are shown in Fig. 4. In the panels for pAl and pFe, profiles from the two stations closest to the South African coast are omitted and plotted separately in Fig. 5.

3.3.1. Biogenic particle distributions: Particulate P, Ca, and Si distributions along I05

Distributions of the biogenic particle tracers in the upper water column indicate two regions of high productivity along the I05 transect. First, high pP concentrations (>15 nM) are observed at stations within 20 km of South Africa, reflecting productive coastal waters in the strong upwelling regime of the Agulhas Current system. Additionally, at two stations over 97–98°E, low sea-surface temperatures, shallow mixed layer depths, and increased phosphate and nitrate concentrations in the mixed layer indicate the presence of a cold-core eddy (Grand et al., 2015a, their Fig. 4). At these same stations, pP (8–10 nM) and pCa (130–150 nM) concentrations are significantly elevated and suggest enhanced coccolithophore productivity within the eddy.

Outside of coastal and eddy-influenced stations, concentrations of pP are generally low (<5 nM) across the interior of the South Indian subtropical gyre. The relatively small north-south range of the I05 cruise track (30–34°S) does traverse a region of sharp gradients in primary

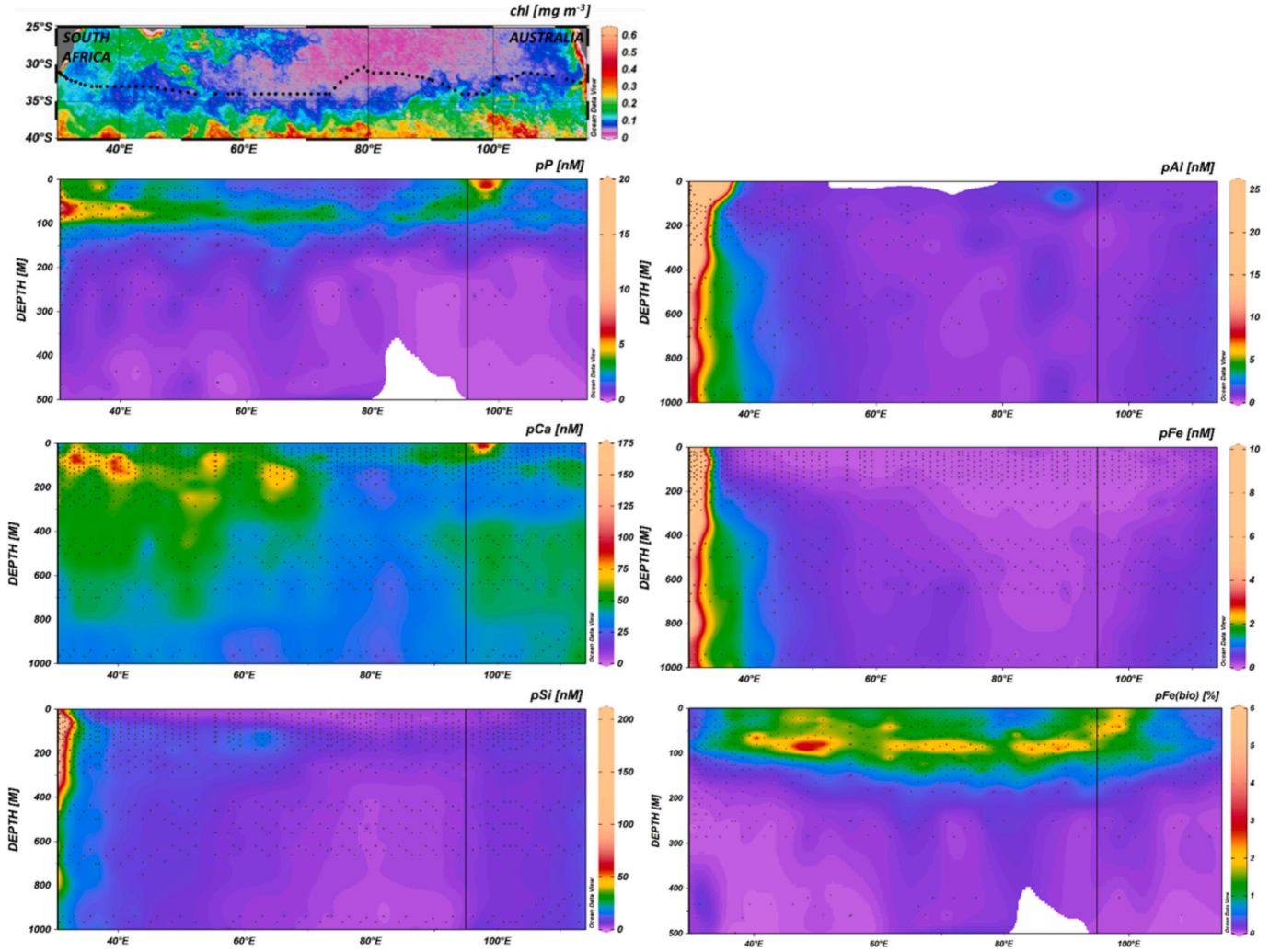

Fig. 4. Distribution of particulate P, Ca, Si, Al, Fe (nM) and pFe_{bio} (%) along CLIVAR section I05. Note the reduced depth scale (500 m) in the plots of particulate P and pFe_{bio}. Black points indicate individual samples; the black line at 95°E represents the crossover point with CLIVAR section I09N/I08S. The top panel shows average chlorophyll concentrations (mg m^{-3}) over March–May 2009 from SeaWiFS satellite imagery overlaid with the locations of trace metal sampling stations.

productivity as shown by average surface-ocean chlorophyll concentrations over March–May 2009 (Fig. 4). Concentrations of pP in the eastern basin exhibit more variability than in the western gyre; these zonal variations can be largely explained by excursions of the I05N cruise track equatorward into the low-productivity gyre interior at ~80°E and ~ 105°E. Similarly, surface-ocean pCa concentrations are relatively constant across the basin (45 ± 18 nM) but decline at ~80°E and ~ 105°E as the I05 transect skirts the edge of the band of high coccolithophore productivity encircling the Southern Ocean from ~30°S to 60°S (Balch et al., 2011; Sadeghi et al., 2012). Concentrations of pSi are generally low through the gyre (typically <25 nM) and are typically highest in the upper 200 m, consistent with biogenic material. However, much higher pSi concentrations (1.0–1.5 μM) are found between the surface and 400 m at stations closest to the African shelf, reflecting lithogenic particles mobilized by the Agulhas Current system over the African shelf, as discussed below.

3.3.2. *Particulate Al and Fe along I05*

Measurable pAl concentrations above the ED-XRF detection limit (0.36 nM) occurred in 41% (n = 405) of suspended particulate matter samples collected along I05 in the South Indian subtropical gyre. Concentrations of pFe were measurable by ED-XRF (>0.02 nM) in 99% of suspended particulate matter samples. Regions with pAl below the detection limit were largely from areas of high-resolution sampling in near-surface waters (<80 m) in the central gyre (50–80°E) and from some intermediate depths at 80–100°E. The low pAl concentrations found in near-surface waters along I05 in the central gyre likely reflect expected low seasonal dust fluxes to the surface ocean. Seasonal back trajectory analyses suggest that transport of dust-laden air masses from the Australian continent, the primary input of Al to surface waters along I05, occurs during austral fall and winter (Grand et al., 2015b). Hence, the bulk of annual deposition of aerosol Al to the subtropical gyre likely occurred 8–9 months prior to sampling along I05. Although the dAl signal from partial dissolution of these mineral aerosols persists (Grand et al., 2015a), pAl is expected to have a shorter residence time in the upper ocean (days to months) (Barrett et al., 2015 and references therein). Hence, short residence times combined with seasonality in aerosol dust supply account for the low pAl concentrations in the surface layer at the time of sampling.

Concentrations of pFe were uniformly low (0.03–0.15 nM) in the upper 200 m of the water column throughout the central South Indian gyre. Vertical profiles of pFe generally display a characteristic subsurface minimum (<0.1 nM) at depths of 50–150 m, coincident with the depth of the subsurface fluorescence maximum and where pFe_{bio} makes up a higher proportion of the total pFe pool (Fig. S4). Biologically-mediated aggregate formation and export leads to efficient vertical transport of lithogenic particles out of the upper water column; these processes have been previously identified as controlling similar features

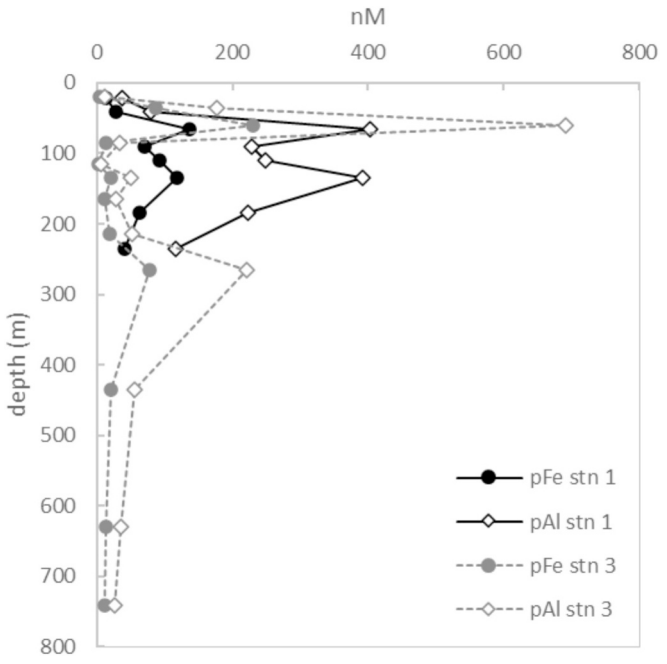

Fig. 5. Profiles of pFe (solid dots) and pAl (open diamonds) at CLIVAR I05 stations 1 (solid lines; 31.065°N, 30.353°E; bottom depth 271 m) and 3 (dashed lines; 31.067°N, 30.410°E; bottom depth 1219 m) approximately 10 km and 15 km, respectively, from the South African coast.

in pFe profiles observed in the subtropical North Atlantic (Barrett et al., 2012).

Both continental margins were observed to supply lithogenic particles to subsurface waters into the interior of the South Indian subtropical gyre. On the eastern edge of the I05 section, transport of shelf sediments along the Australian continental margin results in slightly elevated pAl (1–2 nM) and pFe (0.4–0.9 nM) below 200 m at 12 stations within 1300 km of the coast. The two stations closest to the South African coast reach extremely high pAl (700 nM) and pFe (200 nM) concentrations in the upper water column (Fig. 5). We hypothesize this signal is likely due to vigorous sediment resuspension over the shelf within the Agulhas current, which experiences seasonal peak transport speeds over our sampling period (Feb-March) (Hutchinson et al., 2018). Elevated subsurface pAl (>1 nM) and pFe (>0.4 nM) extend into the interior of the gyre to ~60°E where particle transport into the western gyre is presumably aided by the retroflection of the Agulhas current. After being enriched in shelf-derived particles, these waters flow eastward as the Agulhas Return Current at 39–44°S (Lutjeharms and Ansorge, 2001). Approximately a third of this flow volume is recirculated into the western gyre interior between 40 and 50°E, and another third by 60–70°E. Speeds observed within the southern Agulhas Current (up to ~2 m s^{-1}) and Agulhas Return Current (0.2–1.5 m s^{-1}) (Lutjeharms, 2007) would imply timescales for particle transport of ~1–4 weeks at 40°E to ~3–20 weeks at 60°E.

Towards the center of the basin, there are 5 stations at 34°S between 70 and 74°E with elevated pFe (this work) and dFe (Grand et al., 2015a) at intermediate depths (600–700 m) (Fig. 6). Here, maximum pFe concentrations reach 0.42–0.94 nM compared to maximum pFe concentrations of 0.30–0.46 nM at stations to the immediate east and west. These particle samples are also enriched in Fe (Fe:Al = 0.96 ± 0.28) relative to the composition of particulate matter in the Agulhas recirculation cell (Fe:Al = 0.45 ± 0.13) or at stations impacted by shelf inputs near the Australian margin east of 100°E (Fe:Al = 0.46 ± 0.04). These Fe-rich particles appear to be associated with a supply of dFe to subsurface waters (Fig. 6 and Fig. S5). Concentrations of dFe at the depths >600 m at these 5 stations (0.44–0.99 nM) are significantly higher ($p < 0.01$, two-tailed t-test) than concentrations over the same depths at 5 adjacent stations to the east and west (0.29–0.64 nM). The source of intermediate-depth pFe and dFe signals in this region is unclear. Although the 2009/2010 Japanese-GEOTRACES section GI04 showed that hydrothermal activity along the central Indian Ridge near the Rodriguez Triple Junction impacts the distribution of dFe in the Central Indian basin to 30°S, hydrothermal influence is restricted to depths of 2000–3500 m (Nishioka et al., 2013). Concentrations of dFe at the 2 hydrothermally-impacted stations along GI04 closest to the area of interest are significantly lower in the upper 1000 m than observed along I05 (Fig. 6). There is some shallow topography (<500 m) associated with

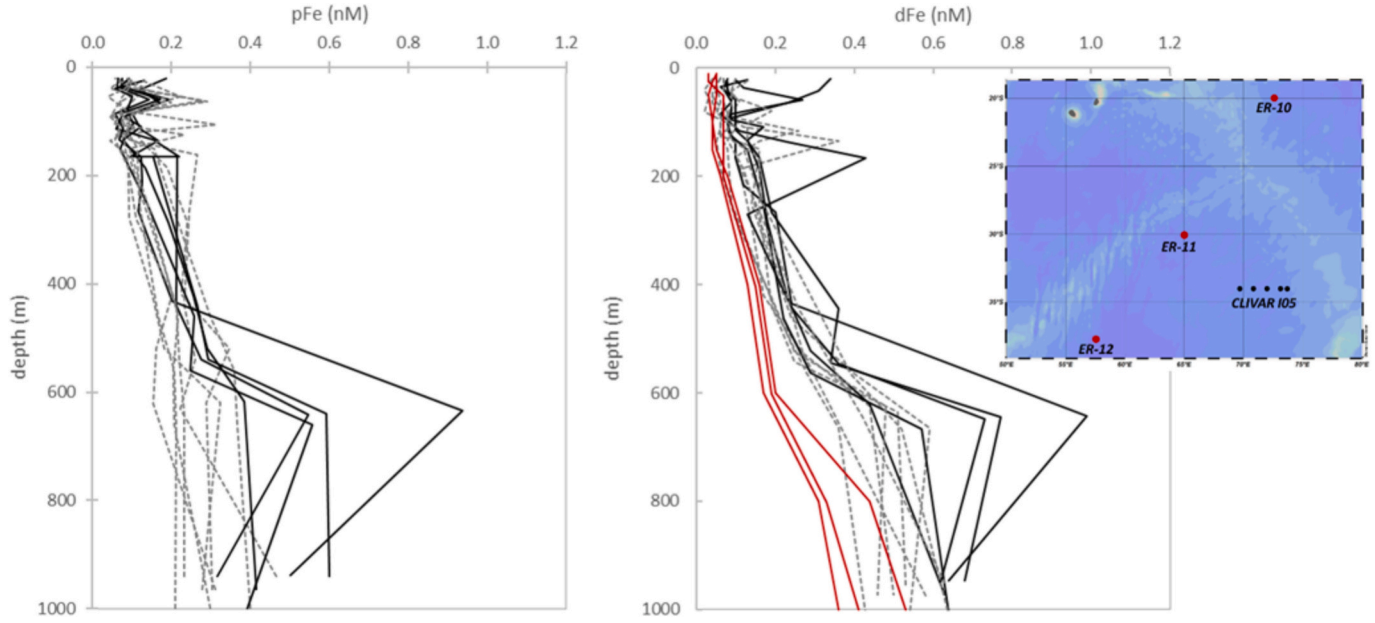

Fig. 6. Profiles of pFe and dFe along CLIVAR I05 at 5 stations over 70–74°E (solid black lines) and compared to adjacent stations to the east and west (66°E–78°E) (dashed grey lines), and dFe profiles from the 2009/2010 Japanese-GEOTRACES section GI04 stations ER-10, ER-11, and ER-12 (solid red lines). Map insert shows the location of CLIVAR I05N stations of interest (black; this study and Grand et al., 2015a) and GI04 stations (red; Nishioka et al., 2013). (For interpretation of the references to color in this figure legend, the reader is referred to the web version of this article.)

the Southeast Indian Ridge, some possibly volcanic, within ~1000 km of these stations that could be an alternative source of hydrothermal Fe, although helium isotope anomalies have not been observed at these depths (Jenkins et al., 2019). Alternatively, these I05 stations are ~1300 km north of the Kerguelen Plateau, which has been shown to be a supply of Fe-rich particles (Chever et al., 2010; van der Merwe et al., 2015) with long residence times in the upper water column to remote HNLC waters thousands of kilometers downstream (Mongin et al., 2009; Grand et al., 2015c). The Subantarctic Mode Water (SAMW) that occupies the thermocline below 250 m at these stations (Grand et al., 2015a) is formed in the northern branch of the ACC near Kerguelen before being injected in the South Indian subtropical gyre (Koch-Larrouy et al., 2010). The transit time between ventilation sites at 30°S is estimated to be on the order of several years (Koch-Larrouy et al., 2010 and references therein), which is similar to expected residence times for lithogenic particles in the upper 1000 m (Barrett et al., 2015). Release of dFe from sedimentary pFe has been increasingly recognized as an important basin-scale supply mechanism (Jeandel and Oelkers, 2015; Milne et al., 2017) and has been suggested both by in situ observations and determined experimentally (Cheise et al., 2018) from resuspended sediments from the Kerguelen Plateau. However, both long-range transport of sedimentary particles or supply of hydrothermal Fe to the upper water column are at present speculative explanations for these elevated dFe and pFe concentrations.

3.3.3. Data comparison at I05 and I09N/I08S crossover

The I09N/I08S and I05 lines intersect in the eastern South Indian subtropical gyre at 34°S and 95°E. The particulate trace element depth profiles at crossover stations sampled approximately 2 years and 60 km apart are shown in Fig. 7. The most notable differences between occupations are associated with higher primary productivity in this region in 2007. Generally, surface-layer concentrations of the biologically-associated trace elements pP (<4 nM), pCa (<60 nM), and pSi (<6 nM) were lower during I05 (April 2009) than measured pP (up to 12 nM), pCa (up to 150 nM), and pSi (up to 17 nM) at the closest two stations from I09N/I08S (March 2007), consistent with satellite observations of lower average sea surface chlorophyll concentrations in 2009 compared to 2007 (Fig. S6). Changes in pFe and pAl profiles between occupations are also primarily associated with this variability in primary productivity. Lower concentrations of pFe (0.09 nM) and a lower proportion of biogenic Fe (<4%) were observed in the surface layer at I05 compared to the I09N/I08S crossover stations (0.12–0.17 nM; up to 13% pFe_{bio}). The subsurface pFe minimum, a feature resulting from biologically-mediated aggregation and export of particles, is also less pronounced, consistent with a less productive mixed layer. In this region, the distribution of pAl in the surface layer has previously been shown to be strongly influenced by scavenging of dAl onto biogenic particles in productive surface waters (Barrett et al., 2018), with concentrations up to 6 nM observed here in 2007 along I09N/I08S. In 2009 during I05, pAl concentrations were below the analytical detection limit

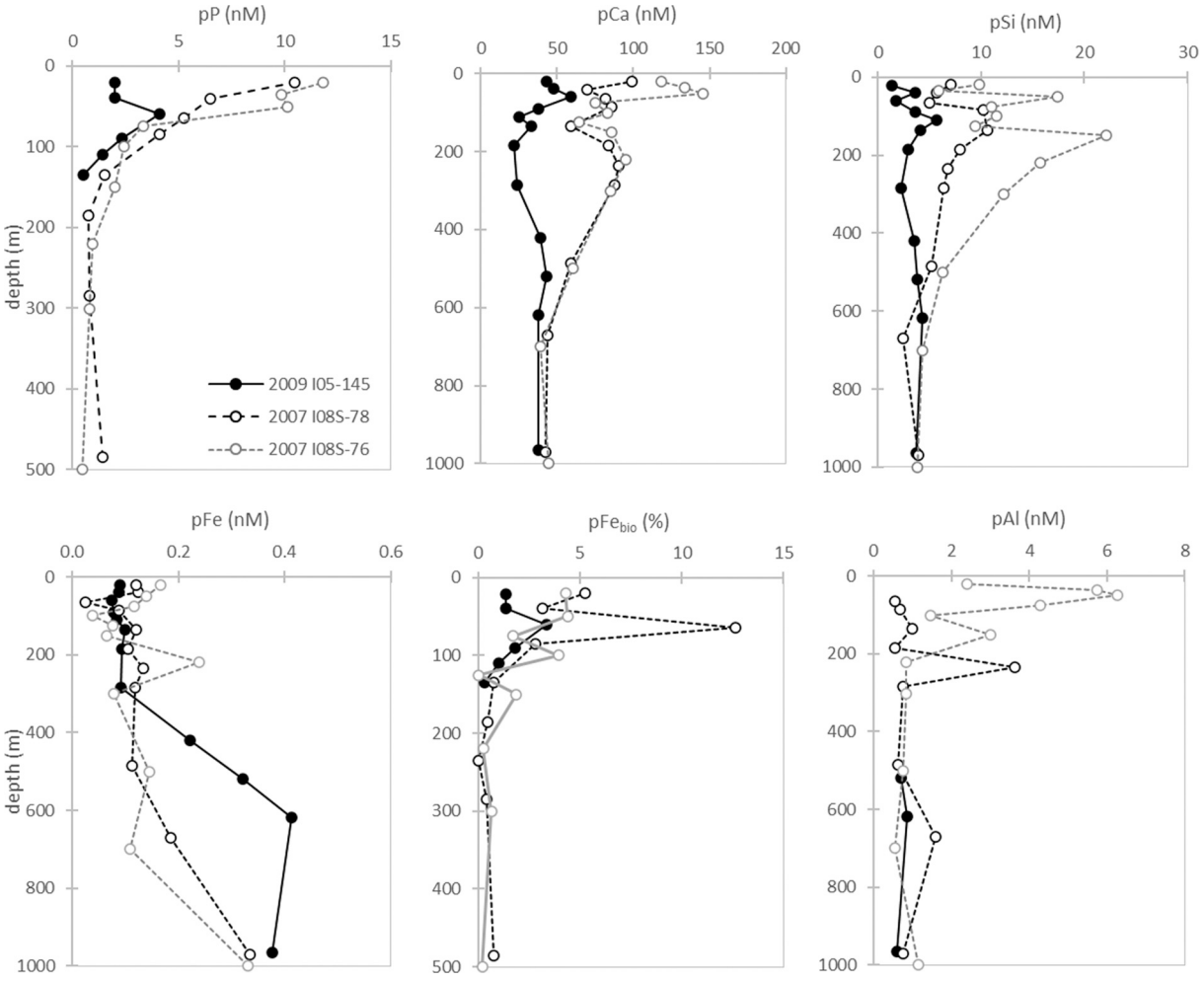

Fig. 7. Vertical profiles of pP, pCa, pSi, pFe, pFe_{bio}, and pAl at CLIVAR I05 station 145 (34.0°S, 95.0°E) sampled on April 29, 2009 (solid symbols) and at CLIVAR I08S stations 78 (33.5°S, 95.0°E) and 76 (34.5°S, 95.0°E) both sampled on March 10, 2007 (open symbols). Note the reduced depth scale (500 m) in the plots of pP and pFe_{bio}; all other plots extend to 1000 m.

in the upper 500 m, consistent with reduced levels biological activity leading to lower scavenging rates of dAl into particles.

4. Conclusions

The I09N/I08S transect illustrates that lithogenic inputs from Ganges-Brahmaputra sediment delivery dominates particle distributions throughout the northern Indian Ocean. The high suspended lithogenic particle load in the Bay of Bengal appears to be important substrate for scavenging subsurface remineralized dFe, as has also been observed in the subtropical North Atlantic (Measures et al., 2008b; Hatta et al., 2014; Barrett et al., 2015). Our observations, taken during peak transport of continental dust flux, suggest that models tend to overestimate trace metal inputs from aerosol deposition over the northern Indian Ocean, consistent with prior in situ data. In the South Indian subtropical gyre, relatively low biological productivity and circulation patterns that carry particles from continental margin input sources into the basin interior mean that lithogenic particles are also the dominant component of the particle flux in the South Indian Ocean. In this regard, the Indian Ocean has similarities to the North Atlantic, although sources that dominate lithogenic particle fluxes in the Indian basin are largely riverine and shelf sediment resuspension rather than primarily mineral dust deposition. We also find evidence of a region in the gyre interior where an unidentified Fe-enriched particle source coincides with observations of elevated dFe concentrations. Both of these signals in the gyre interior potentially indicate a similar mechanism for dFe supply and stabilization as described for shelf-derived particle fluxes in the North Atlantic whereby pFe "buffers" the dFe pool (Milne et al., 2017) by being a reservoir and eventual source of labile Fe. These high-resolution, basin-scale studies provide new insights into lithogenic particle supply and generate trace metal datasets with which to validate biogeochemical model representations.

CRediT authorship contribution statement

Pamela M. Barrett: Writing – original draft, Methodology, Formal analysis. **Joseph A. Resing:** Writing – review & editing, Funding acquisition, Conceptualization. **Maxime M. Grand:** Writing – review & editing, Investigation, Formal analysis. **Christopher I. Measures:** Writing – review & editing, Funding acquisition, Conceptualization. **William M. Landing:** Writing – review & editing, Funding acquisition, Conceptualization.

Acknowledgements

This work was funded by NSF-OCE-0649505, NSF-OCE-2122886, and NSF-OCE-2148091 to JAR, NSF-OCE-0649584 to CIM, and NSF-OCE-0649639 to WML. This is CICOES publication number 2024-1428 and PMEL publication number 5706. We thank the captain and crew of the R/V *Revelle,* and James Swift (UCSD/SIO) and Wilf Gardner (Texas A&M) for generating the CTD and bottle data presented in supporting figures.

Appendix A. Supplementary data

Supplementary data to this article can be found online at https://doi.org/10.1016/j.marchem.2026.104611.

Data availability

Datasets from each section are publicly available on the CCHDO website (http://cchdo.ucsd.edu) under Expocodes 33RR20070322 (I09N), 33RR20070204 (I08S), and 33RR20090320 (I05S).

References

Artigue, L., Wyatt, N.J., Lacan, F., Mahaffey, C., Lohan, M.C., 2021. The importance of water mass transport and dissolved-particle interactions on the aluminum cycle in the subtropical North Atlantic. Glob. Biogeochem. Cycles 35 e2020GB006569.

Balch, W.M., Gordon, H.R., Bowler, B.C., Drapeau, D.T., Booth, E.S., 2005. Calcium carbonate measurements in the surface global ocean based on moderate-resolution imaging Spectroradiometer data. J. Geophys. Res. 110, C07001. https://doi.org/10.1029/2004JC002560.

Balch, W.M., Drapeau, D.T., Bowler, B.C., Lyczskowski, E., Booth, E.S., Alley, D., 2011. The contribution of coccolithophores to the optical and inorganic carbon budgets during the Southern Ocean gas exchange experiment: new evidence in support of the "great Calcite Belt" hypothesis. J. Geophys. Res. 116, C00F06.

Balch, W.M., Drapeau, D.T., Bowler, B.C., Lyczskowski, E.R., Lyczskowski, L.C., Painter, S.C., Poulton, A.J., 2014. Surface biological, chemical, and optical properties of the Patagonian shelf coccolithophore bloom, the brightest waters of the great Calcite Belt. Limnol. Oceanogr. 59, 1715–1732.

Barrett, P.M., Resing, J.A., Buck, N.J., Buck, C.S., Landing, W.M., Measures, C.I., 2012. The trace element composition of suspended particulate matter in the upper 1000 m of the eastern North Atlantic Ocean: A16N. Mar. Chem. 142–144, 41–53.

Barrett, P.M., Resing, J.A., Buck, N.J., Landing, W.M., Morton, P.L., Shelley, R.U., 2015. Changes in the distribution of Al and particulate Fe along A16N in the eastern North Atlantic Ocean between 2003 and 2013: implications for changes in dust deposition. Mar. Chem. 177, 57–68.

Barrett, P.M., Resing, J.A., Grand, M.M., Measures, C.I., Morton, P.L., Landing, W.M., 2018. Trace element composition of suspended particulate matter along three meridional CLIVAR sections in the Indian and southern oceans: impact of scavenging on Al distributions. Chem. Geol. 502, 15–28.

Barua, D.K., Kuehl, S.A., Miller, R.L., Moore, W.S., 1994. Suspended sediment distribution and residual transport in the coastal ocean off the Ganges-Brahmaputra river mouth. Mar. Geol. 120, 41–61.

Buck, C.S., Landing, W.M., Resing, J.A., Measures, C.I., 2010. The solubility and deposition of aerosol Fe and other trace elements in the North Atlantic Ocean: observations from the A16N CLIVAR/CO2 repeat hydrography section. Mar. Chem. 120, 57–70.

Buck, N.J., Barrett, P.M., Morton, P.L., Landing, W.M., Resing, J.A., 2021. Energy dispersive X-ray fluorescence methodology and analysis of suspended particulate matter in seawater for trace element compositions and an intercomparison with high-resolution inductively coupled plasma-mass spectrometry. Limnol. Oceanogr. Methods 19, 401–415.

Chan, C.-Y., Zheng, L., Sohrin, Y., 2024. The behaviour of aluminium, manganese, iron, cobalt, and lead in the subarctic Pacific Ocean: boundary scavenging and temporal changes. J. *Oceanogr*. 80, 99–115.

Cheise, M., Planquette, H.F., Fitzsimmons, J.N., Pelleter, E., Sherrell, R.M., Lambert, C., Bucciarelli, E., Sarthou, G., Le Goff, M., Liorzou, C., Cheron, S., Viollier, E., Gayet, N., 2018. Contribution of resuspended sedimentary particles to dissolved iron and manganese on the ocean: An experimental study. Chem. Geol. 511, 389–415.

Chever, F., Sarthou, G., Bucciarelli, E., Blain, S., Bowie, A.R., 2010. An iron budget during the natural iron fertilization experiment KEOPS (Kerguelen Islands, Southern Ocean). Biogeoscience 7, 455–468.

Chinni, V., Singh, S.K., Bhushan, R., Rengarajan, R., Sarma, V.V.S.S., 2019. Spatial variability in dissolved iron concentrations in the marginal and open waters of the Indian Ocean. Mar. Chem. 208, 11–28.

Dammshäuser, A., Wagener, T., Garbe-Schönberg, D., Croot, P.L., 2013. Particulate and dissolved aluminum and titanium in the upper water column of the Atlantic Ocean. Deep-Sea Res. I 73, 127–139.

GEOTRACES Intermediate Data Product, 2021. (IDP2021). NERC EDS British Oceanographic Data Centre NOC. https://doi.org/10.5285/cf2d9ba9-d51d-3b7c-e053-8486abc0f5fd.

Ginoux, P., Chin, M., Tegen, I., Prospero, J.M., Holben, B., Dubovik, O., Lin, S.-J., 2001. Sources and distributions of dust aerosols simulated with the GOCART model. J. Geophys. Res. 106, 20255–20273.

Grand, M.M., Measures, C.I., Hatta, M., Morton, P.L., Barrett, P.M., Milne, A., Resing, J. A., Landing, W.M., 2015a. The impact of circulation and dust deposition in controlling the distributions of dissolved Fe and Al in the south Indian subtropical gyre. Mar. Chem. 176, 110–125.

Grand, M.M., Measures, C.I., Hatta, M., Hiscock, W.T., Buck, C.S., Landing, W.M., 2015b. Dust deposition in the eastern Indian Ocean: the ocean perspective from Antarctica to the Bay of Bengal. Glob. Biogeochem. Cycles 29, 357–374.

Grand, M.M., Measures, C.I., Hatta, M., Hiscock, W.T., Landing, W.M., Morton, P.L., Buck, C.S., Barrett, P.M., Resing, J.A., 2015c. Dissolved Fe and Al in the upper 1000m of the eastern Indian Ocean: a high-resolution transect along 95°E from the Antarctic margin to the bay of Bengal. Glob. Biogeochem. Cycles 29, 375–396.

Hatta, M., Measures, C.I., Wu, J., Roshan, S., Fitzsimmons, J.N., Sedwick, P., Morton, P., 2014. An overview of dissolved Fe and Mn distributions during the 2010–2011 U.S. GEOTRACES North Atlantic cruises: GEOTRACES GA03. Deep-Sea Res. II 116, 177–129.

Holligan, P.M., Charalampopoulou, A., Hutson, R., 2010. Seasonal distributions of the coccolithophore, Emiliania huxleyi, and of particulate inorganic carbon in surface waters of the Scotia Sea. J. Mar. Syst. 82, 195–205.

Holynska, B., Bisiniek, K., 1976. Determination of trace amounts of metals in saline water by energy dispersive XRF using the NaDDTC preconcentration. J. Radioanal. Nucl. Chem. 31, 159–166.

Hulten, Van, et al., 2017. Manganese in the West Atlantic Ocean in the context of the first global ocean circulation model of manganese. Biogeoscience 14, 1123–1152.

Hutchinson, K., Beal, L.M., Penven, P., Ansorge, I., Hermes, J., 2018. Seasonal phasing of Agulhas current transport tied to a Baroclinic adjustment of near-field winds. J. Geophys. Res. Oceans 123, 7067–7083.
Hydes, D.J., 1979. Aluminum in seawater: control by inorganic processes. Science 205, 1260–1262.
Islam, M.R., Begum, S.F., Yamaguchi, Y., Ogawa, K., 1999. The Ganges and Brahmaputra rivers in Bangladesh: basin denudation and sedimentation. Hydrol. Process. 13, 2907–2923.
Jeandel, C., Oelkers, E.H., 2015. The influence of terrigenous particulate material dissolution on ocean chemistry and global element cycles. Chem. Geol. 395, 50–66.
Jenkins, W.J., Doney, S.C., Fendrock, M., Fine, R., Gamo, T., Jean-Baptiste, P., Key, R., Klein, B., Lupton, J.E., Newton, R., Rhein, M., Roether, W., Sano, Y., Schlitzer, R., Schlosser, P., Swift, J., 2019. A comprehensive global oceanic dataset of helium isotope and tritium measurements. Earth Syst. Sci. Data 11, 441–454.
Jickells, T.D., An, Z.S., Andersen, K.K., Baker, A.R., Bergametti, G., Brooks, N., Cao, J.J., Boyd, P.W., Duce, R.A., Hunter, K.A., Kawahata, H., Kubilay, N., LaRoche, J., Liss, P. S., Mahowald, N.M., Prospero, J.M., Ridgwell, A.J., Tegen, I., Torres, R., 2005. Global iron connections between desert dust, ocean biogeochemistry, and climate. Science 308, 67–71.
Koch-Larrouy, A., Morrow, R., Penduff, T., Juza, M., 2010. Origin and mechanism of Subantarctic mode water formation and transformation in the southern Indian Ocean. Ocean Dyn. 60, 563–583.
Lutjeharms, J.R.E., 2007. Three decades of research on the greater Agulhas current. Ocean Sci. 3, 129–147.
Lutjeharms, J.R.E., Ansorge, I.J., 2001. The Agulhas return current. J. Mar. Syst. 30, 115–138.
Mahowald, N.M., Baker, A.R., Bergametti, G., Brooks, N., Duce, R.A., Jickells, T.D., Kubilay, N., Prospero, J.M., Tegen, I., 2005. Atmospheric global dust cycle and iron inputs to the ocean. Glob. Biogeochem. Cycles 19, GB4025.
Measures, C.I., Landing, W.M., Brownand, M.T., Buck, C.S., 2008a. A commercially available rosette system for trace metal-clean sampling. Limnol. Oceanogr. Methods 6, 384–394.
Measures, C.I., Landing, W.M., Brown, M.T., Buck, C.S., 2008b. High-resolution Al and Fe data from the Atlantic Ocean CLIVAR-CO_2 repeat hydrography A16N transect: extensive linkages between atmospheric dust and upper ocean geochemistry. Glob. Biogeochem. Cycles 22, GB1005.
Menzel Barraqueta, J.-L., Klar, J.K., Gledhill, M., Schlosser, C., Shelley, R., Planquette, H. F., Wenzel, B., Sarthou, G., Achterberg, E.P., 2019. Atmospheric deposition fluxes over the Atlantic Ocean: a GEOTRACES case study. Biogeoscience 16, 1525–1542.
Milne, A., Schlosser, C., Wake, B.D., Achterberg, E.P., Chance, R., Baker, A.R., Forryan, A., Lohan, M.C., 2017. Particulate phases are key in controlling dissolved iron concentrations in the (sub)tropical North Atlantic. Geophys. Res. Lett. 44, 2377–2387.
Mongin, M.M., Abraham, E.R., Trull, T.W., 2009. Winter advection of iron can explain the summer phytoplankton bloom that extends 1000 km downstream of the Kerguelen Plateau in the Southern Ocean. J. Mar. Res. 67, 225–237.
Moran, S.B., Moore, R.M., 1988. Temporal variations in dissolved and particulate aluminum during a spring bloom. Estuar. Coast. Shelf Sci. 27, 205–215.
Murtugudde, R.G., Signorini, S.R., Christian, J.R., Busalacchi, A.J., McClain, C.R., Picaut, J., 1999. Ocean color variability of the tropical indo-Pacific basin observed by SeaWiFS during 1997-1998. J. Geophys. Res. 104, 18351–18366.
Nishioka, J., Obata, H., Tasumune, D., 2013. Evidence of an extensive spread of hydrothermal dissolved iron in the Indian Ocean. Earth Planet. Sci. Lett. 361, 26–33.
Orians, K.J., Bruland, K.W., 1986. The biogeochemistry of aluminum in the Pacific Ocean. Earth Planet. Sci. Lett. 78, 397–410.
Panda, P.P., Shukla, G., Kumar, A., Aswini, M.A., Kaushik, A., Nayak, G., Matta, V.M., 2014. Atmospheric deposition of mineral dust and associated nutrients over the equatorial Indian Ocean. Sci. Total Environ. 915, 169779.
Sadeghi, A., Dinter, T., Vountas, M., Taylor, B., Altenburg-Soppa, M., Bracher, A., 2012. Remote sensing of coccolithophore blooms in selected oceanic regions using the PhytoDOAS method applied to hyper-spectral satellite data. Biogeoscience 9, 2127–2143.
Schott, F.A., Dengler, M., Shoenefeldt, R., 2002. The shallow overturning circulation of the Indian Ocean. Prog. Oceanogr. 53, 57–103.
Sedwick, P.N., Church, T.M., Bowie, A.R., Marsay, C.M., Ussher, S.J., Achilles, K.M., Lethaby, P.J., Johnson, R.J., Sarin, M.M., McGillicuddy, D.J., 2005. Iron in the Sargasso Sea (Bermuda Atlantic time-series study region) during summer: Eolian imprint, spatiotemporal variability, and ecological implications. Biogeochem. Cycles 19, GB4006.
Somes, C.J., Dale, A.W., Wallmann, K., Schlotz, F., Yao, W., Oschlies, A., Muglia, J., Schmittner, A., Achterberg, E.P., 2021. Constraining global marine iron sources and ligand-mediated scavenging fluxes with GEOTRACES dissolved Iron measurements in an ocean biogeochemical model. Glob. Biogeochem. Cycles 35 e2021GB006948.
Srinivas, B., Sarin, M.M., 2013. Atmospheric dry-deposition of mineral dust and anthropogenic trace metals to the bay of Bengal. J. Mar. Syst. 126, 56–68.
Stramma, L., Lutjeharms, J.R.E., 1997. The flow field of the subtropical gyre of the South Indian Ocean. J. Geophys. Res. 102, 5513–5530.
Stummeyer, J., Marchig, V., Knabe, W., 2002. The composition of suspended matter from Ganges–Brahmaputra sediment dispersal system during low sediment transport season. Chem. Geol. 185, 125–147.
Twining, B.S., Baines, S.B., 2013. The trace metal composition of marine phytoplankton. Annu. Rev. Mar. Sci. 5, 191–215.
Twining, B.S., Rauschenberg, S., Baer, S.E., Lomas, M.W., Martiny, A.C., Antipova, O., 2019. A nutrient limitation mosaic in the eastern tropical Indian Ocean. Deep-Sea Res. II. https://doi.org/10.1016/j.dsr2.2019.05.001.
van der Merwe, P., Bowie, A.R., Quéroué, F., Armand, L., Blain, S., Chever, F., Davies, D., Dehairs, F., Planchon, E., Sarthou, G., Townsend, A.T., Trull, T.W., 2015. Sourcing the iron in the naturally fertilised bloom around the Kerguelen plateau: particulate trace metal dynamics. Biogeoscience 12, 739–755.
van Hulten, M.M.P., Sterl, A., Tagliabue, A., Dutay, J.-C., Gehlen, M., de Baar, H.J.W., Middag, R., 2013. Aluminium in an ocean general circulation model compared with the West Atlantic Geotraces cruises. J. Mar. Syst. 126, 3–23.
Weber, et al., 2018. Biological uptake and reversible scavenging of zinc in the global ocean. Science 361, 72–76.
Wedepohl, K.H., 1995. The composition of the continental crust. Geochim. Cosmocim. Acta 59, 1217–1232.
Xu, H., Weber, T., 2021. Ocean dust deposition rates constrained in a data-assimilation model of the marine aluminum cycle. Glob. Biogeochem. Cycles 35 e2021GB007049.
Ye, Y., Völker, C., 2017. On the role of dust-deposited Lithogenic particles for Iron cycling in the tropical and subtropical Atlantic. Glob. Biogeochem. Cycles 31, 1543–1558.
Ye, Y., Wagener, T., Volker, C., Guieu, C., Wolf-Gladrow, D.A., 2011. Dust deposition: iron source or sink? A case study. Biogeoscience 8, 2107–2124.
Zender, C.S., Bian, H., Newman, D., 2003. Mineral dust entrainment and deposition (DEAD) model: description and dust climatology. J. Geophys. Res. 104, 4416.
Dutay, et al., 2015. Modelling the role of marine particle on large scale ^{231}Pa, ^{230}Th, Iron and Aluminium distributions. Prog. Oceanogr. 133, 66–72.
Tagliabue, et al., 2016. How well do global ocean biogeochemistry models simulate dissolved iron distributions? Glob. Biogeochem. Cycles 32, 149–174.